

# Intuitive Teleoperation of Active Catheters for Endovascular Surgery

B. Rosa<sup>1\*</sup>, A. Devreker<sup>1\*</sup>, H. De Praetere<sup>2</sup>, C. Gruijthuijsen<sup>1</sup>, S. Portoles-Diez<sup>1</sup>,  
 A. Gijbels<sup>1</sup>, D. Reynaerts<sup>1</sup>, P. Herijgers<sup>2</sup>, J. Vander Sloten<sup>1</sup>, E. Vander Poorten<sup>1</sup>

**Abstract**—Advances in miniature surgical instrumentation are key to less invasive and safer medical interventions. In cardiovascular procedures interventionalists turn towards catheter-based interventions, treating patients considered unfit for classical more invasive approaches. Improvements in design and steerability of catheters could further reduce the invasiveness of these interventions. For example, by improving controllability and interaction forces with the vessels, tissue damage could be limited. Through improved steerability and coordinated control, operation times and exposure to radiation might also be reduced. Latter argument formed the original motivation for the development of teleoperated robotic catheters. Despite the large kinematic dissimilarity and thus non-trivial mapping between joystick input and catheter output motion, few investigations have been conducted to find intuitive mappings that allow straightforward catheter steering. This paper presents some recent work in this direction. Three promising mappings are proposed. The mappings were implemented and validated upon a robotic catheter moving inside an artificial aorta model. Experimental results show good steerability of the robotic catheter for all the mappings. Although superiority of one mapping with respect to the others was observed, further investigation and validation is planned. In the future, additional visual cues that increase the situational awareness of the user are expected to further simplify the steering.

## I. INTRODUCTION

Reducing invasiveness of surgical techniques is a major concern in the medical community. In cardiac surgery, this has led to a whole new set of interventions based on catheters. Thanks to technological improvements, patients with high peri-operative risks suffering from severe aortic stenosis, that were previously classified as inoperable, can now be treated using a trans-catheter approach: Transcatheter Aortic Valve Implantation (TAVI) [1]. In the transfemoral TAVI approach (Fig.1), a catheter, guidewires and sheaths are introduced into the femoral artery and navigated through the vascular system until the catheter can be positioned in the center of the diseased aortic valve. In a first step the original aortic valve is dilated by inflating a catheter-embarked balloon, in a second step the valve implant is brought into place and implanted. Depending on the patient anatomy and stenosis status, transfemoral and transapical routes for valve implantation are considered as complementary. This paper focuses on the transfemoral approach.

Transfemoral TAVI is minimally invasive for the patient but presents considerable challenges for the surgeon and risks

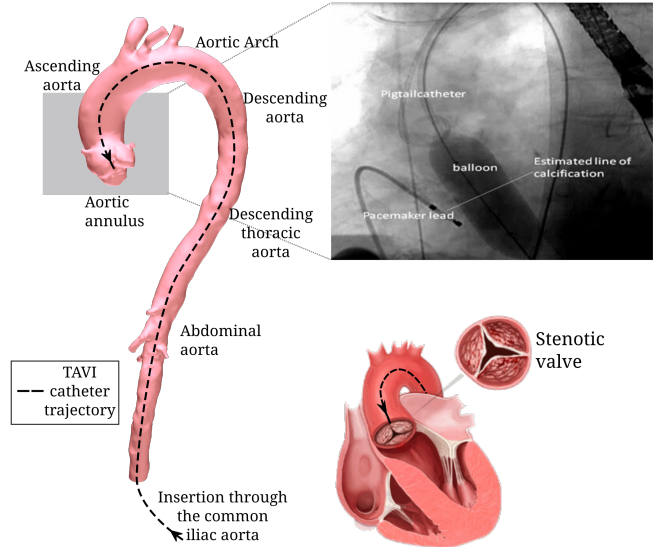


Fig. 1. Transcatheter Aortic Valve Implantation; [left] aortic anatomy, trajectory followed by valve placement catheter; [right-up] fluoroscopic image of aortic annulus, balloon dilation to make place for valve implant; [bottom-right] view upon stenotic aortic valve.

for the patient. Current catheters and instruments are difficult to control in this dynamic environment. The procedure therefore takes longer than necessary and more importantly the patient is overly exposed to radiation and to contrast agent [2]. For instance the NovaFlex+ Transfemoral System (Edwards Lifescience, USA) only provides a single manually controllable distal bending motion that must be combined with manual insertion and rotations of the entire catheter. Every placement step of the guidewires, supporting sheaths, and valve delivery catheters is done under X-ray guidance. Also, because of lack of maneuverability, the risk of plaque disruption, puncture of tissue and tissue damage form an important concern for TAVI surgeries [3], [4].

The introduction of robotic technology in the cardiac operating room creates expectations to improve endovascular procedures [5], [6]. Although a number of commercial robotic systems already exist for endovascular surgery, amongst others systems produced by Hansen Medical, Corindus and Stereotaxis, none of them are intended for TAVI [5]. Moreover, coordinated control of the distal degrees of freedom is difficult due to the limited and unequal dynamic response of these systems. This explains the difficulty to deploy these devices for operation in dynamic environments such as close to the aortic annulus [7].

<sup>1</sup> KU Leuven, Department of Mechanical Engineering, 3001 Leuven, Belgium [firstname.lastname@kuleuven.be](mailto:firstname.lastname@kuleuven.be)

<sup>2</sup> Department of Experimental Cardiac Surgery, University Hospital Leuven, 3000 Leuven, Belgium [first.second@uzleuven.be](mailto:first.second@uzleuven.be)

\* B. Rosa and A. Devreker contributed equally to this study

These matters have drawn the attention from the research community, and various active catheters have been developed. Though most of those systems make use of tendon actuation [8], [9], [10], magnetic steering systems [11], fluidic actuation [12], [13], and shape memory alloys [14], have been explored in the past. The authors have been developing pneumatic catheters with McKibben pneumatic artificial muscles [13]. Hydraulic actuation has not yet been considered for integration simplicity reasons. The design of the active catheter, though being described in the present paper, is however not the main focus of this study.

Robotic catheter systems offer an enhanced manoeuvrability at the tip, and allow the surgeon to operate remotely, outside the reach of damaging X-ray radiation. The surgeon typically gives steering commands through an input joystick. Specific joystick motions are mapped to individual catheter/guidewire motions. In current commercial systems the surgeon has to toggle additional buttons to select an adequate mapping that gives him/her access to the appropriate catheter DoFs. This way of operation requires a considerable learning curve [15]. Through development of *coordinated* control approaches, whereby surgeons can command multiple DoFs simultaneously, learning curves could potentially be shortened. Due to the dissimilar kinematics of the robotic catheter and the master input devices, it is however not trivial to come up with mappings that allow intuitive and efficient operation of the different catheter DoFs (Degrees of Freedom). The optimal solution will likely also depend on the specific surgical task and anatomy.

This paper presents three intuitive mappings that can be used to steer a distally actuated catheter through the vasculature (in a femoral TAVI operation). Section II presents the experimental setup: a 4-DoF haptic master interface that is used to steer a pneumatically actuated robotic catheter. Section III presents and discusses three mappings to control the tip movements of the robotic catheter using the said haptic interface. Experiments are carried out on a realistic replica of the aorta. The aim of these experiments is to assess the practicality and intuitiveness of the different mappings (section IV). The paper ends in section V with conclusions that are drawn from the present study and some elements for further work.

## II. COMPONENTS FOR ROBOTIC TRANSCATHETER AORTIC VALVE IMPLANTATION

This section presents the active catheter and teleoperation setup that was designed and built for robotic execution of TAVI procedures. The *proximal* DoFs are the insertion/retraction motion of the catheter and the rotation about its longitudinal axis. They are actuated proximally at the level of the entry-port. These DoFs correspond to the traditional DoFs that are available to the surgeon when manually steering catheters. As these DoFs affect the entire pose and shape of the catheter, they are also referred to as *global* DoFs. A catheter driver for these DoFs is briefly discussed in subsection II-A.1. In subsection II-A.2 an actuation mechanism to control the *distal* motion, *local* w.r.t. the catheter

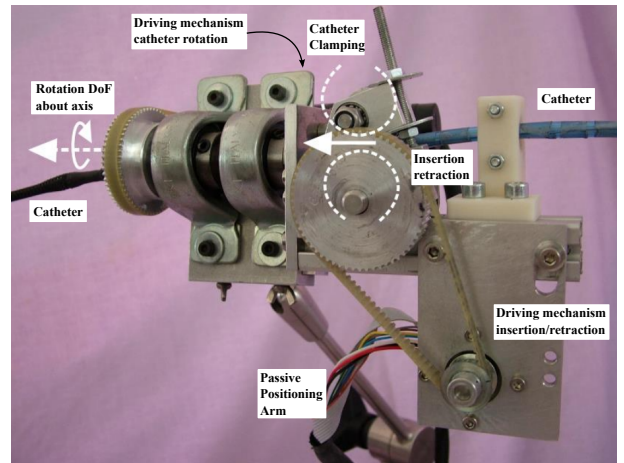


Fig. 2. View on 2-DoF catheter driver for global actuation. The catheter passes through the pair of bearings in the frontal part of the device. The pairs of rollers are in charge of the translation. The entire ensemble rotates around its axis (collinear with catheter axis).

tip, is discussed. A 4-DoF haptic joystick that has been selected to steer the ensemble of catheter DoFs is discussed in subsection II-B.1. Through a dedicated software platform (subsection II-B.2) all components are linked, actuators and sensors are controlled (subsection II-B.3) and processed in real-time. This setup forms the basis of the research towards intuitive coordinated control of catheters (section III).

### A. Design of a multi-DoF robotic catheter

1) *Catheter driver for proximal actuation:* A simple catheter driver has been used to control the two proximal (*global*) catheter DoFs. Fig. 2 shows a picture of this driver loaded with an in-house developed catheter. The driver makes use of two friction rollers which can be tensioned manually to accommodate for different catheter diameters (from 3 to 10mm) and adjust the clamping force. A brushless DC-motor (Maxon EC-i 40 Ø40mm, 50W) and belt transmission are used to drive one of the rollers. The pairing roller is not actuated and passively follows the motion of the catheter. The assembly consisting of roller pair, clamping mechanism and linear motion driving unit is rotated together with the catheter about an axis collinear with the catheter's longitudinal axis. This is achieved by hinging the assembly in a pair of bearings located at one extremity of the device. By doing so we can keep a maximal rotational range not affected by cable windup. A hollow shaft passes through the axis of the bearing pair. The catheter moves through this hollow shaft. At one end the shaft carries the linear motion assembly, at the other end it connects via a transmission belt (not visible in the picture) to a second DC-motor (Maxon A-max 26 Ø26mm, 11W). This motor then rotates the ensemble of hollow shaft, catheter and translation stage. Table I reviews the main features of this system.

2) *Fluidic distal actuation:* Rather than tendon-driven actuation, this study makes use of purposely-designed pneumatic actuation to steer the catheter's distal DoFs. Pneumatic

TABLE I  
PERFORMANCE OF THE CATHETER DRIVER

linear stroke	$\infty^{(*)}$	incremental accuracy	< 0.1 mm
rotational stroke	$\infty^{(*)}$	rotational accuracy	0.1 degree
diameter range	3 to 10mm	output force	10N
bandwidth	> 5Hz		

(\*) in practice limited by the catheter length  
(\*) in practice limited by twisting of the power supply cables

artificial muscles are characterized by a high force to volume ratio, while having the advantage of being inherently compliant [13]. Here, McKibben muscles are employed and embedded in the distal section of the catheter. The distal part of the developed pneumatic catheter is presented in Fig. 3. It consists of four muscles that are symmetrically distributed around an axi-symmetric tension spring that acts as a return spring. The bending motion of the actuated segment is achieved by pressurizing one or a combination of artificial muscles. The length differences between the pressurized muscles and the return spring determines the curvature and the bending orientation of the local actuator. The entire distal segment is 60mm long and has an external diameter of 7mm. Each muscle is made in-house with a balloon placed inside a braided sheath. The muscles are 50mm long and have, at rest, a diameter of 2.1mm and a braid angle of 28°. The central tension spring has a diameter of 0.9mm. The described structure achieves a maximal bending angle of 50° when pressurizing a single muscle at 5 bars. The developed catheter also possesses an electromagnetic (EM) position sensor (6DoF Aurora sensor, NDI Medical, Canada) fixed at its tip for tracking purposes (see Fig. 3).

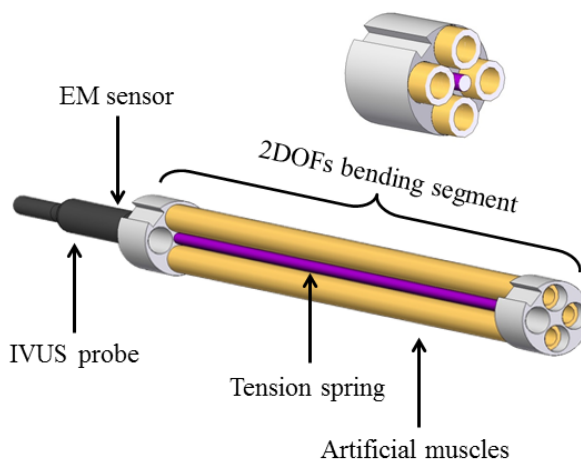


Fig. 3. CAD design of the catheter bending segment. One of the four muscles of the bending segment is omitted for clarity. A cross section at a connection piece is also presented. The black part at the catheter tip represents an intra-vascular ultrasound (IVUS) probe (Visions PV 8.2 by Volcano Corporation). The EM position sensor is fixed inside the IVUS probe lumen. In the present work, only the electromagnetic tracker is used, but parallel developments directed at online 3D reconstruction use both the IVUS and the EM data [19].

State-of-the-art cable-actuated mechanisms suffer from

friction and/or backlash between cable and cable-guide along the catheter length. Such phenomena limit the achievable positioning precision and dynamics of the distal actuation. Noteworthy efforts a.o. by Kesner *et al.* [8] have been conducted to model and compensate for this friction. However, as the friction and backlash vary with the catheter shape and interaction with the vessel wall, it is clear that compensation has its limits. One advantage of pneumatic actuation is that the pressure supply lines that run along the length of the catheter body are only marginally affected by variations of the catheter shape and interactions with the vessel walls. Precise control of the tip is then only limited by the non-linear behaviour exhibited by McKibben muscles [16], [17], [18]. In this study, hysteresis was not considered, and a constant ratio linking pressure to bending angle was used for controlling the tip movements. Indeed, since the surgeon closes the control loop, rather than absolute positioning accuracy, only relative positioning precision is needed. On the condition that the actuator bandwidth is sufficiently high to follow surgeons commands and an intuitive mapping is offered, the surgeon should then be able to compensate for the non-idealities him/herself and achieve superior positioning performance.

Although the characteristics of the proposed catheter are not optimized for clinical practice (an outer diameter equivalent to current valve delivery instrument, such as the 6mm NovaFlex+ Transfemoral System, is desired), the catheter suffices for investigating the intuitive control and mappings in an aorta model, which forms the main scope of this study. Further research will look towards optimization of the active catheter. This would entail further miniaturisation to achieve a smaller outer diameter and allowing for a working channel. Note that such working channel would not be used for transferring the valve implant as we envision to load it directly at the tip of the distal section, but could e.g. be used to pass a guide-wire or a pressure line to expand the valve implant.

#### B. Teleoperation system for coordinated catheter control

1) *Haptic joystick for catheter steering:* An in-house developed 4-DoFs haptic joystick [20], depicted in Fig.4, was selected to steer the different catheter DoFs. The joystick was originally designed for general MIS applications, but seems also very much suited for controlling robotic catheters. The device has 3 rotational DoFs (roll  $\psi$ , pitch  $\theta$  and yaw  $\phi$ ) that orient the joystick end-effector (handle) about one fixed point in space. A 4<sup>th</sup> DoF allows translational motion  $r$  of the handle through this point and in a direction parallel to the longitudinal axis of the handle. Table II summarizes the main characteristics of this device. Whereas the translational DoF  $r$  is naturally destined to command the insertion/retraction motion of the catheter (in rate-control), it is not that straightforward how the three rotational DoFs  $\psi$ ,  $\theta$ ,  $\phi$  are to be mapped.

2) *Software framework:* The robotic catheter and haptic joystick were interfaced with the CASCADE software platform. This is a dedicated surgical robotic control platform

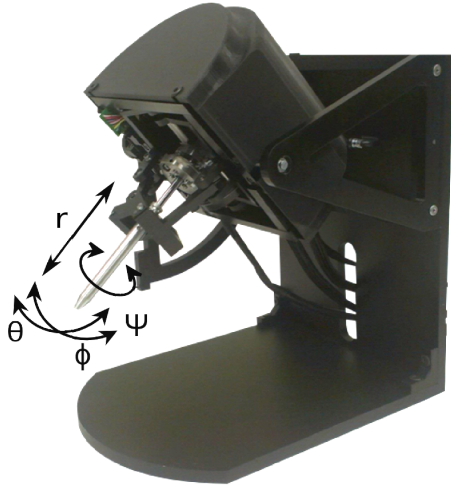


Fig. 4. Four DoF haptic joystick with single translational DoF  $r$  and three rotational DoFs  $\psi$  the rotation about the axis of the handle and  $\phi$  and  $\theta$  for rotation about a unique center of motion. The origin of the joystick frame  $\Sigma_{joy}$  is coinciding with this central point.

TABLE II  
MAIN CHARACTERISTICS OF 4-DOF HAPTIC JOYSTICK[20]

	$r$	$\psi$	$\theta$	$\phi$
range	[30 – 80]mm	210deg	90deg	$[\pm 25 - 85]^{(1)}$
resolution	$\leq 1.5\mu\text{m}$	$\leq 0.24\text{deg}$	$\leq 9\mu\text{ deg}$	$\leq 16\mu\text{ deg}$
cont.force/torque	$\geq 22\text{N}$	44mNm	$\geq 11\text{N}^{(2)}$	$\geq 11\text{N}^{(2)}$

<sup>(1)</sup> lower bound for  $r \rightarrow 80\text{mm}$

<sup>(2)</sup> equivalent forces at the tip of the handle

that is developed in the framework of the EU-funded FP7 project CASCADE. The platform links OROCOS for hard real-time robotic control [21], with ROS for messaging and non-realtime tasks. It further includes Qt and OpenCV for graphical interfaces and visualisation.

3) *Low-level control of the different components:* The haptic joystick is controlled at 1kHz generating a crisp virtual wall informing the user when he/she is reaching the limits of the catheter's workspace. Gravity compensation is implemented in order to improve the transparency of the device. A spring-damper with a dead-zone is implemented in the radial direction ( $r$ -axis). Precise control over the catheter insertion/retraction speed is possible through rate-control along this DoF. The motors of the proximal catheter driver are controlled in torque for insertion/retraction and rotation of the catheter. A pressure controller is used to actuate the bending DoFs. The pressure in the McKibben muscles is controlled through a set of four servo-valves (FESTO MPPES-3-1/4-10-010). The controller outputs an analog voltage for each of the servo-valves. 0V corresponds to atmospheric pressure, while 5V corresponds to maximal pressure (5 bars). Note that in this study, air is used. In clinical practice hydraulic actuation using saline would be an option as it avoids risk of embolization. Also the employed pressure level corresponds to levels that are typically being used in low-pressure endovascular applications such as in

molding or occlusion ballooning. A description of a similar actuation principle has been reported by Devreker *et al.*[22].

### III. INTUITIVE STEERING OF ACTIVE CATHETERS

This section presents the mappings that have been developed in search for an intuitive catheter control. The user-controlled variables are the joystick angles ( $\psi$ ,  $\theta$ , and  $\phi$ ) and insertion  $r$ . The different mappings, depicted in Fig.5, link these variables to the torques  $\tau_i$  and  $\tau_r$  applied by the insertion and rotation motor respectively, and to the pressure in the McKibben muscles  $\beta$  (along  $\mathbf{e}_x^t$ ) and  $\gamma$  (along  $\mathbf{e}_y^t$ ) (see Fig. 6 for definitions of  $\mathbf{e}_x^t$  and  $\mathbf{e}_y^t$ ). Note that positive values for  $\beta$  (resp.  $\gamma$ ) correspond to bending along  $\mathbf{e}_x^t$  (resp  $\mathbf{e}_y^t$ ), whereas negative values cause bending in the  $-\mathbf{e}_x^t$  (resp  $-\mathbf{e}_y^t$ ) direction. Common to all mappings is that the insertion/retraction is controlled by the translational joystick DoF ( $r$  in Fig. 4), using a rate control. This is expressed as  $\tau_i \propto (r - r_0)$ , where  $\propto$  denotes a proportional relation.

#### A. Mapping 1: direct joint-based control

Mapping 1 (M1) is depicted in Fig. 5a. It was designed so that the hand movements of the user correspond to the manual gestures a surgeon would perform during current TAVI procedures. There is thus a direct joint mapping:

$$\begin{cases} \tau_r & \propto \psi \\ \beta & = \frac{\theta}{\theta_{max}} \\ \gamma & = \frac{\phi}{\phi_{max}} \end{cases} \quad (1)$$

The mapping translates the rotation of the joystick ( $\psi$ ) to a rotation of the catheter driver, using a rate control.  $\theta$  and  $\phi$  are mapped to the two antagonistic pairs of the McKibben muscles at the tip of the catheter. The subscript  $max$  indicates the maximal angle that can be reached on the joystick axis. While this mapping seems to be intuitive because it is close to current practice, the controllability of the catheter rotation about its axis is rather low, due to the low catheter torsional stiffness. As a result, the function  $f$  (defined in Fig. 5), linking the joystick roll  $\psi$  and the achieved tip rotation  $\alpha$  is unknown and probably highly non-linear, making it difficult for the operator to estimate the tip rotation  $\alpha$ . Also in reality this rotational DoF is particularly difficult to control. Note that the tip rotation determines in which planes the antagonistic McKibben muscles will lie. As such it will also determine in which direction yaw and pitch bending will take place. The fact that the overall rotation angle  $\alpha$  is unknown to the operator complicates the steering. The operator will need thus to continuously estimate  $\alpha$  to determine appropriate yaw and pitch steering commands. This might result in non-functional probing commands in order to understand the current catheter orientation.

#### B. Mapping 2: distal bending plane and amplitude control

Whereas M1 might suffer from the unpredictability of the catheter torsion  $\alpha$ , mapping 2 (M2) gives the user the possibility to compensate for this catheter torsion him/herself. The basic idea behind M2 is to redefine the control over the

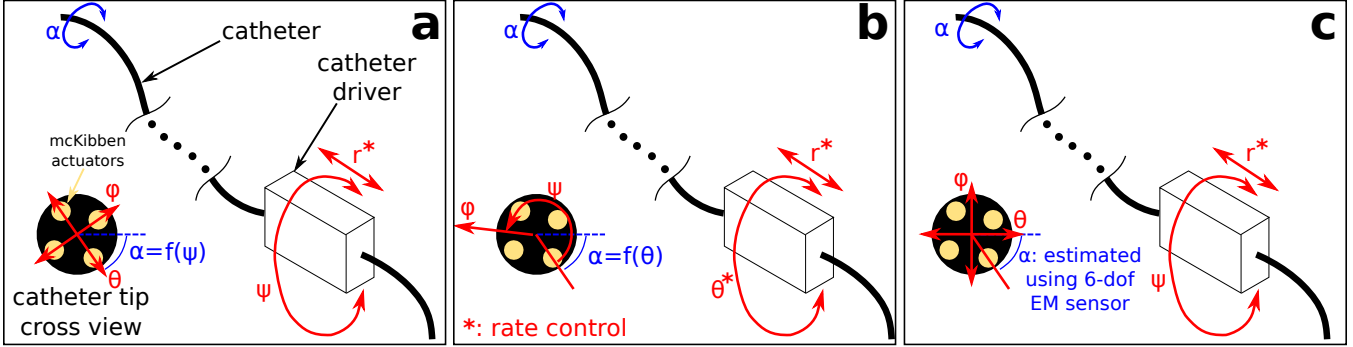


Fig. 5. Schematic description of the 3 mappings.  $r, \theta, \phi$  and  $\psi$  refer to the DoF of the master joystick (see Fig. 4)

pairs of antagonistic McKibben muscles in a way such that orienting the catheter's bending plane and bending in this bending plane, i.e. the bending amplitude, are decoupled. The orientation of the bending plane is controlled by the angle  $\psi$  on the joystick. The bending amplitude is mapped to the joint angle  $\phi$ . This mapping is represented in Fig. 5b. Finally, the proximal rotation is mapped to the angle  $\theta$ . A rate control scheme is used for the latter. This allows the user to maximally keep the joystick aligned with the vertical axis. It is expected that such might allow for a more accurate control over the bending amplitude. In summary, this is described as:

$$\begin{cases} \tau_r & \propto \theta \\ \beta & = \frac{\phi}{\phi_{max}} \cos(\psi) \\ \gamma & = \frac{\phi}{\phi_{max}} \sin(\psi) \end{cases} \quad (2)$$

A possible additional advantage of such mapping could be that it would allow the user to precisely adjust the bending orientation while keeping the bending amplitude constant. Such behaviour could be particularly advantageous when crossing the aortic arch which is known to have an approximately constant curvature. A possible drawback could exist in a relatively large learning curve due to the difference with normal surgical practice.

### C. Mapping 3: direct control with torsion compensation

Mapping 3 (M3) is depicted in Fig. 5c. It is largely similar to M1, except that the catheter's torsional component is automatically compensated for. For this we make use of direct measurement of the catheter's tip orientation (and estimation of the angle  $\alpha$ ) through the 6-DoF EM sensor integrated in the catheter tip (see Fig. 3). From this knowledge the torsional rotation is then compensated for so that the catheter tip always bends in the direction that the operator is indicating with the haptic master:

$$\begin{cases} \tau_r & \propto \psi \\ \beta & = \frac{\theta}{\theta_{max}} \cos(\alpha) - \frac{\phi}{\phi_{max}} \sin(\alpha) \\ \gamma & = \frac{\theta}{\theta_{max}} \sin(\alpha) + \frac{\phi}{\phi_{max}} \cos(\alpha) \end{cases} \quad (3)$$

Note that M3 effectively cancels out any proximal rotational motion imposed by the catheter driver. In fact this

might be one of the greatest advantages of this mapping, as rotational motion of the catheter about its axis induces intense contacts with large surfaces of the vessel wall. Such motions could induce tissue damage or cause dislodgement of plaque or calcifications which often arise in the targeted patient groups.

The rotation angle  $\alpha$  is estimated as follows: first, a plane  $\pi$  is constructed based on vector  $\mathbf{e}_z^t$  belonging to the tip coordinate frame  $\Sigma_t$  and collinear with the catheter centerline at the catheter tip, and a vector  $\mathbf{u}$  in the direction of gravity (see Fig. 6 left). Then, a control coordinate system  $\Sigma_c$  is defined as follows. The z-axis is aligned with  $\mathbf{e}_z^t$ , thus  $\mathbf{e}_z^t = \mathbf{e}_z^c$ ; vector  $\mathbf{e}_x^c$  is computed as  $\frac{\mathbf{u} \times \mathbf{e}_z^t}{\|\mathbf{u} \times \mathbf{e}_z^t\|}$ ;  $\mathbf{e}_y^c$  is then found so as to form an orthonormal base. The angle  $\alpha$  is then found as the rotational angle between  $\mathbf{e}_x^t$  and  $\mathbf{e}_x^c$  about  $\mathbf{e}_z$  (see Fig. 6 right). Note that  $\mathbf{e}_y^c$  is most of the times distinct from  $\mathbf{u}$ : they are equal only when the catheter's tip is perfectly horizontal.

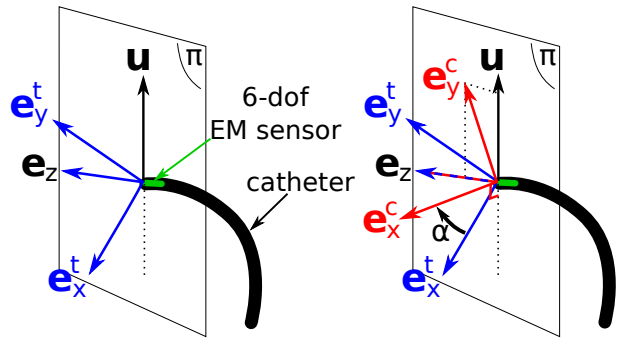


Fig. 6. Estimation of the tip rotation  $\alpha$  of the catheter, defined as the rotation angle around  $\mathbf{e}_z$  between the bases  $(\mathbf{e}_x^t, \mathbf{e}_y^t, \mathbf{e}_z^t)$  (EM sensor frame) and  $(\mathbf{e}_x^c, \mathbf{e}_y^c, \mathbf{e}_z^c)$ . By construction  $\mathbf{e}_z^t = \mathbf{e}_z^c$ .

## IV. EXPERIMENTS

### A. Experimental setup

Fig. 7 gives an overview of the experimental setup. The catheter is passed in the catheter driver and positioned in front of a 1:1 scale silicone aorta model (T-S-N-001-1, Elastrat, Switzerland). Next to it, the haptic joystick is positioned so that the user can see the progress of the insertion of the catheter inside the model. Finally, under the model is the

field generator of the electromagnetic tracking system (NDI Aurora) that allows to track the tip of the catheter both in orientation and position in the whole aorta. During the experiments, both the haptic joystick and the catheter driver are placed outside of the NDI Aurora measurement volume in order to avoid electromagnetic interferences. Since the materials used in the catheter are medical grade stainless steel and aluminium, and the speed of displacement of the tip is typically a few mm/s, one can expect a measuring accuracy of 0.5 mm from the Aurora system [23].

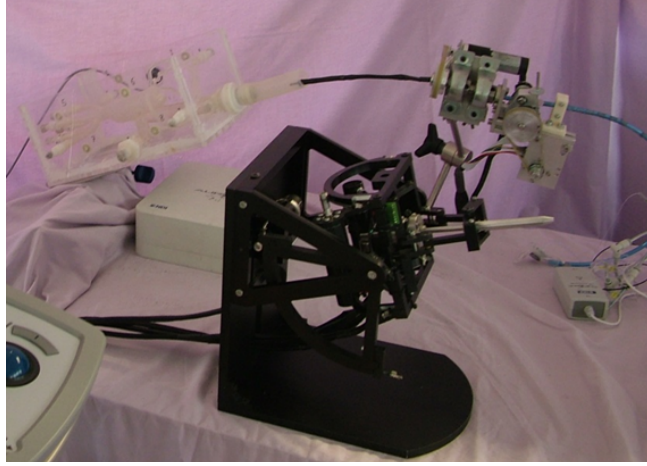


Fig. 7. Picture of the teleoperation system that was built up showing the respective components: haptic joystick, proximal catheter driver, IVUS tower, aorta model and structure with fluidic muscles for distal actuation

The testing protocol consists in carrying out introductions of the robotic catheter inside the aorta model to the aortic valve. The user is first instructed about the different mappings and given an unlimited amount of time to get acquainted with the different mappings, doing several insertions. When the user is ready, the experiment is started. The full experiment contains 6 series. Each series consists of 8 insertions performed with a given mapping, of which only the last five insertions are recorded. The recording starts and stops at the subject's call, when he starts moving the catheter and when he reaches the aortic valve, respectively. When the five insertions are finished, another series begins with a different mapping. The order of the mappings is randomized in order to avoid an experimental bias owing to this order. During the experiments, the user is looking directly at the model in order to see the position of the catheter in the vasculature, which is of course not possible in real procedures. This simplification was introduced in order to have the user focus solely on the mappings and intuitive control.

#### B. Objective assessment of performance

In order to objectively assess the performance of the users that perform the task, the following metrics are used.

$T_f$  is the time to finish the task. This does not include the fine movements needed for reaching the center of the aortic valve, which will be investigated in details in a next study.

TABLE III

RESULTS OF THE STATISTICAL ANALYSIS

Metric	$p_{KW}$	$p_U^{1-2}$	$p_U^{2-3}$	$p_U^{1-3}$
$T_f$	0.03	0.03	<0.01	0.26*
$L_p$	0.01	0.02	<0.01	0.17*
$\eta_{sal}$	0.03	0.03	<0.01	0.45*
$p_v$	<0.01	0.1*	<0.01	<0.01

\* Non-significant p-values

TABLE IV

MEDIAN AND INTERQUARTILE RANGE OF THE METRICS

Metric	Median			IQR		
	M1	M2	M3	M1	M2	M3
$T_f(s)$	18.1	11.0	18.9	13.5	6.9	5.6
$L_p(cm)$	37.04	29.80	39.66	16.3	4.2	5.0
$\eta_{sal}$	-17.9	-9.2	-15.4	13.7	5.6	6.4
$p_v$	0.70	0.72	0.52	0.12	0.13	0.06

$L_p$  is the arc length of the path followed by the tip of the catheter, from the starting point to the end of the trajectory. It is estimated using the EM sensor integrated in the tip.

$\eta_{sal}$  is the smoothness of the path followed by the tip of the catheter (again, estimated using the EM data). It is calculated using the spectral arc length method that computes the length of the spectral arc of the spectrum of the speed profile for a given movement [24]. This method has recently been shown to be highly correlated to the expertise of endovascular surgeons [25]. The method is robust, adimensional, speed- and time-independent.  $\eta_{sal}$  is a negative number: the higher (closer to zero) it is, the smoother the movement is.

$p_v$  is the variance explained by the first component of the principal component analysis conducted on the pressure inside the pneumatic valves. It is representative of the usage made by the subject: if this value is high, it means that the subject is not making full use of the capabilities of the catheter and uses mainly one bending direction. On the contrary, if the value is low it means that the subject uses the different bending directions. Note that the directions are in the catheter's tip frame  $\Sigma_t$ .

#### C. Results

One expert endovascular surgeon carried out the full series of tests, i.e. 30 insertions inside the aorta after an unrecorded training with the device. Since the normality of the data cannot be assumed, the Kruskal-Wallis test –the non-parametric equivalent of the ANOVA– was used to assess the statistical difference between the three mappings. If the p-value was found significant ( $< 0.05$ ), the Mann-Whitney U-test was used as a post-hoc test to determine which of the mappings were statistically different one to another (with a bonferroni correction of the p-value in order to compensate for repeated testing).

The results are summarized in Table III (statistical tests, where  $p_{KW}$  is the p-value of the Kruskal-Wallis test and  $p_U^{i-j}$  is the following post-hoc U-test between mappings  $i$  and  $j$ ) and table IV (median and interquartile range of the different metrics for the three mappings). As a comparison, the ‘ideal’

path consisting of following the centerline of the vessel has a length of 28.9 cm (computed from the 3D model of the aorta used in this study, using the 3-matic software from Materialise, Belgium). With a constant speed of 20 mm/s, this would lead to a completion time of 14.49 seconds.

M2 seems to be the best mapping in terms of completion time  $T_f$ , length of path  $L_p$  and smoothness  $\eta_{sal}$ . This is an interesting result as M2 was not expected to be the most intuitive mapping at first. The user also indicated to be positively surprised by this mapping. Skeptical at first, the surgeon's confidence about the mapping grew within a few minutes and mentioned explicitly that it felt easy to use.

More surprising is the absence of statistically significant differences between M1 and M3 regarding completion time, length of path and smoothness of movements. This could be explained by the fact that the user is an expert endovascular surgeon. We observed that the surgeon -in accordance to his normal practice/experience, was constantly trying to use the rotation of the whole catheter for progressing in the aorta (see Fig. 8). Since in M3 the tip rotation  $\alpha$  is compensated for at all times it followed that the progression was more difficult and chaotic. This is consistent with the values of  $p_v$ , which are significantly lower for M3 with respect to the two other mappings: since the user was rotating the catheter at the proximal side constantly, the different muscles were used more evenly than in the two other mappings.

## V. CONCLUSION

This paper presents control strategies for intuitive navigation of an active catheter in the aorta for TAVI surgery. The catheter has two distal degrees of freedom that are actuated by McKibben mini-actuators. The actuators allow a sufficient bending angle in order to navigate in the aorta. The catheter is teleoperated by means of a haptic joystick, and inserted/rotated at its base by a catheter driver.

Three mappings between the DoFs of the joystick and the catheter DoFs are proposed for intuitive control of the catheter. M1 is a direct joint-based mapping that is quite similar to current manual practice. M2 is a distal spherical joint mapping. The mapping allows independent selection of the bending plane of the catheter tip from selection of the bending amplitude. M3 is similar to the first mapping, but possesses some compensation action to compensate for possible twist of the catheter around its axis while progressing along the vasculature. It was conceived to overcome the uncontrollable catheter twist that causes disorientation and as such complicates the catheter steering.

Experiments were carried out by an expert endovascular surgeon; these consisted of multiple insertions in a flexible aorta model. The experiments show that the user is better performing with M2, both in terms of time to reach the aortic valve ( $p=0.03$ ), length of path ( $p=0.01$ ) and smoothness of the movements ( $p=0.03$ ). Despite looking more complicated at first, this mapping allows easy selection of the rotation angle for crossing the aortic arch. This property was appreciated very much by the user (after a certain learning period). It is also interesting to note that, although M3 seems

to be the most intuitive at first, the user experienced problems operating with this mapping because of his habitual actions originating from manual practice. The surgeon tends to make heavy use of the catheter proximal rotation despite the fact that this action is compensated for in M3.

Further work will be directed towards more extensive validation of the teleoperation setup with a larger population of experts. A further study will look at the use of 3D rendering of the catheter tip position in a pre-operatively acquired 3D model of the patient vasculature (constructed from CT images), together with information extracted from the IVUS data. Further research will also be conducted to develop a second version of the actuator with a smaller outer diameter. Characterization of the dynamic response and hysteresis of the distal actuators will also be studied.

## ACKNOWLEDGEMENT

Research funded by the European Commission 7th Framework Programme FP7-ICT - Under grant agreement No 601021, EU project CASCADE

## REFERENCES

- [1] R. R. Makkar, G. P. Fontana, H. Jilaihawi, S. Kapadia, A. D. Pichard *et al.*, "Transcatheter aortic-valve replacement for inoperable severe aortic stenosis," *New England Journal of Medicine*, vol. 366, no. 18, pp. 1696–1704, 2012.
- [2] A. M. Kasel, S. Cassese, A. W. Leber, W. von Scheidt, and A. Kastrati, "Fluoroscopy-guided aortic root imaging for TAVR: 'Follow the Right Cusp' rule," *JACC: Cardiovascular Imaging*, vol. 6, no. 2, pp. 274 – 275, 2013.
- [3] J. Plotkin, R. Siegel, and R. Beigel, "Plaque disruption during transcatheter aortic valve replacement," *Eur Heart J. Cardiovasc. Imaging*, vol. 15, no. 1, pp. 117–117, Jan 2014.
- [4] A. Aminian, J. Lalmand, and B. El Nakadi, "Perforation of the descending thoracic aorta during transcatheter aortic valve implantation (tavi): An unexpected and dramatic procedural complication," *Catheterization and Cardiovascular Interventions*, vol. 77, no. 7, pp. 1076–1078, 2011.
- [5] J. Bonatti, G. Vetrovec, C. Riga, O. Wazni, and P. Stadler, "Robotic technology in cardiovascular medicine," *Nature Reviews Cardiology*, vol. 11, no. 5, pp. 266–275, 2014.
- [6] H. Rafii-Tari, C. J. Payne, and G.-Z. Yang, "Current and emerging robot-assisted endovascular catheterization technologies: A review," *Annals of biomedical engineering*, vol. 42, no. 4, pp. 697–715, 2014.
- [7] G. Srinathveeravalli, T. Kesavadas, and X. Li, "Design and fabrication of a robotic mechanism for remote steering and positioning of interventional devices," *The International Journal of Medical Robotics and Computer Assisted Surgery*, vol. 6, no. 2, pp. 160–170, 2010.
- [8] S. Kesner and R. Howe, "Position control of motion compensation cardiac catheters," *Robotics, IEEE Transactions on*, vol. 27, no. 6, pp. 1045–1055, 2011.
- [9] ———, "Robotic catheter cardiac ablation combining ultrasound guidance and force control," *The International Journal of Robotics Research*, 2014.
- [10] G. J. Vrooijink, T. T. Ellenbroek, P. Breedveld, J. G. Grandjean, and S. Misra, "A preliminary study on using a robotically-actuated delivery sheath (rads) for transapical aortic valve implantation," in *IEEE Int. Conf. Robot. Autom. (ICRA'14)*, 2014, pp. 4380–4386.
- [11] Y. Fu, H. Liu, W. Huang, S. Wang, and Z. Liang, "Steerable catheters in minimally invasive vascular surgery," *The International Journal of Medical Robotics and Computer Assisted Surgery*, vol. 5, no. 4, pp. 381–391, 2009.
- [12] K. Ikuta, H. Ichikawa, K. Suzuki, and D. Yajima, "Multi-degree of freedom hydraulic pressure driven safety active catheter," in *Robotics and Automation, 2006. ICRA 2006. Proceedings 2006 IEEE International Conference on*, May 2006, pp. 4161–4166.

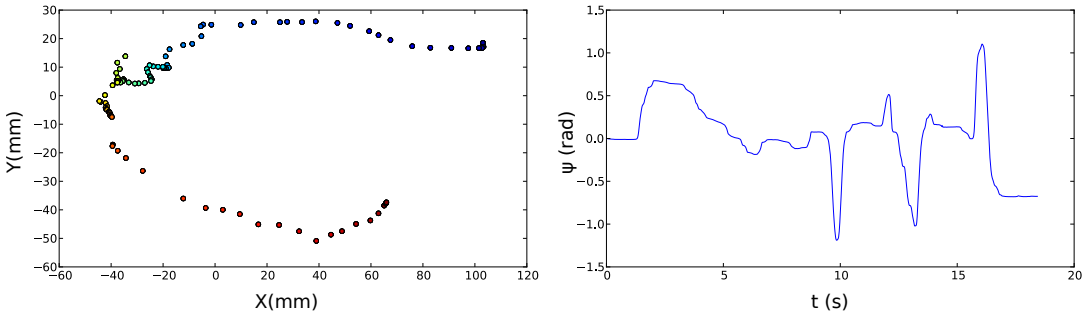


Fig. 8. Example of insertion with M3. Left: followed path of the catheter tip, projected on the principal plane of the aorta (beginning in blue, end of trajectory in red). Right: usage of the  $\psi$  angle of the joystick, controlling the rotation of the catheter driver

- [13] A. Devreker, E. Vander Poorten, P. Tran, H. De Praetere, P. Herijgers, J. Vander Sloten, and D. Reynaerts, "Towards fluidic actuation for catheter-based interventions," in *Proceedings Actuator 2014*, Bremen, Germany, 2014, pp. 173–176.
- [14] J. Jayender, R. V. Patel, and S. Nikumb, "Robot-assisted active catheter insertion: algorithms and experiments," *The International Journal of Robotics Research*, vol. 28, no. 9, pp. 1101–1117, 2009.
- [15] C. Riga, C. Bicknell, R. Sidhu, F. Cochenne, P. Normahani, P. Chadha, E. Kashef, M. Hamady, and N. Cheshire, "Advanced catheter technology: Is this the answer to overcoming the long learning curve in complex endovascular procedures," *European Journal of Vascular and Endovascular Surgery*, vol. 42, no. 4, pp. 531 – 538, 2011. [Online]. Available: <http://www.sciencedirect.com/science/article/pii/S1078588411000694>
- [16] B. Tondu and P. Lopez, "Modeling and control of mckibben artificial muscle robot actuators," *Control Systems, IEEE*, vol. 20, no. 2, pp. 15–38, 2000.
- [17] E. G. Hocking and N. M. Wereley, "Analysis of nonlinear elastic behavior in miniature pneumatic artificial muscles," *Smart Materials and Structures*, vol. 22, no. 1, p. 014016, 2013.
- [18] C. S. Kothera, M. Jangid, J. Sirohi, and N. M. Wereley, "Experimental characterization and static modeling of mckibben actuators," *Journal of Mechanical Design*, vol. 131, no. 9, p. 091010, 2009.
- [19] C. Shi, S. Giannarou, S.-L. Lee, and G.-Z. Yang, "Simultaneous catheter and environment modeling for trans-catheter aortic valve implantation," in *Intelligent Robots and Systems (IROS 2014), 2014 IEEE/RSJ International Conference on*, Sept 2014, pp. 2024–2029.
- [20] A. Gijbels, E. Vander Poorten, P. Stalmans, H. Van Brussel, and D. Reynaerts, "Design of a teleoperated robotic system for retinal surgery," in *IEEE International Conference on Robotics and Automation*, 2014.
- [21] H. Bruyninckx, P. Soetens, and B. Koninckx, "The real-time motion control core of the Orococos project," in *IEEE International Conference on Robotics and Automation*, 2003, pp. 2766–2771.
- [22] A. Devreker, B. Rosa, A. Desjardins, E. Alles, L. Garcia-Peraza, E. Maneas, D. Stoyanov, A. David, T. Vercauteren, J. Deprest, S. Ourselin, D. Reynaerts, and E. Vander Poorten, "Fluidic actuation for intra-operative in situ imaging," in *Intelligent Robots and Systems (IROS 2015), 2015 IEEE/RSJ International Conference on*, 2015.
- [23] C. Nafis, V. Jensen, L. Beauregard, and P. Anderson, "Method for estimating dynamic em tracking accuracy of surgical navigation tools," in *Medical Imaging*. International Society for Optics and Photonics, 2006, pp. 61410K–61410K.
- [24] S. Balasubramanian, A. Melendez-Calderon, and E. Burdet, "A robust and sensitive metric for quantifying movement smoothness," *IEEE Trans. Biomed. Eng.*, vol. 59, no. 8, pp. 2126–2136, 2012.
- [25] S. J. Estrada, "Quantitative movement analysis in endovascular surgical tasks for objective determination of skill," Ph.D. dissertation, Doctoral Thesis, Rice University, 2014.